JOURNAL OF COMPUTATIONAL PHYSICS 25, 133–150 (1977)

New Three-Dimensional Simulation Models for Cylindrical and Toroidal Plasmas

C. Z. CHENG AND H. OKUDA

Plasma Physics Laboratory, Princeton University, Princeton, New Jersey 08540

Received July 12, 1976; revised November 17, 1976

A new class of three-dimensional particle simulation models using finite-size particles has been developed which is useful for studying plasma behavior in large, cylindrical, and toroidal systems. The model makes use of the combination of eigenfunction expansion in one direction and the multipole expansion on a two-dimensional spatial grid for solving the Maxwell equations and for pushing particles. For a toroidal system, the Poisson equation is solved by using the cubic spline technique in the radial direction. It is shown that, using presently available computers, full three-dimensional simulations may be carried out for real plasma devices such as tokamaks or pinch devices where only several eigenmodes are required in the axial direction. Results of the simulations for the thermal fluctuations are shown to agree with the theoretical predictions for both cylindrical and toroidal systems.

1. INTRODUCTION

Since the pioneering work on one-dimensional models by Buneman [1] and Dawson [2], the particle simulatin of plasmas has been in continuous progress as the need increases for understanding the nonlinearities and many-body properties associated with plasma dynamics. Nonlinear behavior of various microinstabilities, plasma heating associated with the parametric instabilities and plasma diffusion due to convective cells, are some of the examples in which the particle simulation played a decisive role for understanding of the physical processes involved.

Recently, it has been recognized that the particle simulation method can also be very useful in more applied fields of plasma physics directly aimed at the controlled nuclear fusion research. Some of these examples are the simulations of neoclassical diffusion [3], neutral beam injection processes in a tokamak [4], and the impurity sputtering from the wall [5]. For these calculations, self-consistent electric and magnetic fields are usually ignored and the particle orbits are followed in three dimensions for a given electric and magnetic fields. For many cases, Monte Carlo method is employed to model the interactions among particles through the Fokker–Planck collision operator.

Most of the self-consistent simulations have been carried out in an idealized system in reduced dimensions. To avoid the interaction with the boundary, periodic boundary conditions are often employed to simulate an infinite system. Furthermore, unrealistic mass ratios are used so as to shorten the computing time. While consider-

ISSN 0021-9991

581/25/2-5

able progress has been made for simulating a plasma with realistic parameters in a bounded, finite length system using realistic mass ratios [6], possibilities of simulating a full three-dimensional large plasma device has not been much pursued so far.

In this paper we will explore the possibility of simulating large, three-dimensional cylindrical and toroidal plasmas using a hybrid approach of spatial grid and eigenfunction expansion technique for solving the Maxwell equations and for pushing particles. In Section 2, the model is introduced for a cylinder and a torus of rectangular cross section. For a toroidal system we have developed a finite-size particle model retaining up to the dipole terms, and the radial Poisson equation is solved by cubic spline technique. Tests of the models are shown in Section 3 including the measurements of the thermal spectrum. Concluding remarks are given in Section 4.

2. Model

1. *Basic Ideas For The Model*

It is well known that, for particle simulation of plasmas, there are two major kernels which are most important and also most time consuming. One of them is to solve the Maxwell equations for the electric and magnetic fields. The other is to push the particles according to the equation of motion.

When one deals with the one-dimensional model where the plasmas are represented by a group of positively and negatively charged sheets, the solution of Maxwell equations is indeed trivial [1, 2, 7]. The electrostatic field, for example, is constant everywhere except at the particle location where it jumps by the amount of $4\pi\rho$ across a sheet where ρ is the surface charge density. It is sufficient to count the number of positive and negative sheets for determining the electrostatic field. When a sheet crosses the other sheet during the course of its motion, the electric field on the sheet changes suddenly giving rise to the short-range collisional effects as opposed to collective effects due to the ordered motion of many particles. It is well known that the collisional effects in one dimension is small.

For two-dimensional simulations, the electrostatic field, for example, generated by a two-dimensional charged rod varies as $1/r$ where r is the distance from the charge and the observer. In contrast to one dimension, the field becomes very large and varies very rapidly when two particles come close enough with each other. In other words, the two-dimensional collisional effects are overwhelmingly large so that it can wipe out the collective effects easily as was seen in some of the initial effort for the two-dimensional simulations.

The great success of the use of finite-size particles lies in the fact that one can disregard the short-range force in a most natural way by assuming a particle has finite size comparable to the Debye length, thus eliminating the short-range, two-body interactions. Further smoothing is carried out when the force on an extended particle is calculated by using a spatial grid. Here, instead of calculating the exact force on a particle, an approximate force is calculated using the electric and magnetic

fields defined on the spatial grid points [8]. It was found that this procedure is equivalent to the multipole expansion in electrodynamics [9].

There are also several examples, where the same technique is extended successfully to a full three dimensions using a three-dimensional spatial grid [10, 11]. While this model is very efficient in calculating the electric and magnetic fields and the force on a particle, one cannot simulate a large volume of plasma due to the limited capacity of the available computers. Due to the grid instabilities [12, 13], the Debye length should not be smaller than a fraction of grid size Δ, say, one-half of Δ. Let us assume, for example, one can simulate a system of $64 \times 64 \times 64$ grid using a presently available large scientific computer. Assuming an optimum size of grid, say $\Delta = 2\lambda_D$, the physical size of the system would then be $128 \times 128 \times 128$ Debye cube. Let us compare the size of this simulation with the size of existing real plasma devices. A Q-machine [14], which is typically used for basic plasma research, has a plasma dimension of 1–2 cm radius by 50–100 cm long. This would imply a plasma to be a size of 100–200 Debye length across by 5×10^4 Debye length long. Therefore, the simulation plasma is large enough for the cross section while it is much too short in the axial direction. Similar conclusions can be drawn for larger fusion devices such as tokamaks or stellarators where the length in the toroidal direction is much longer than the cross-sectional length. This simply indicates that it is not possible to simulate real devices using a most advanced scientific computer to date. Needless to say, one would like to keep the grid quantities such as electric and magnetic fields in the central core of a computer while keeping the particle data in the outside device such as disks. Because of the fact that the grid quantities are randomly accessed, transferring the large grid in and out between disks and main cores would be painfully time consuming, and we should consider some other way to save the situation.

While the axial length of the real devices is much longer than the dimension of a cross section, we know theoretically and by laboratory experiments that most of the important physics for plasma confinement are associated with the modes of very long wavelength along the field lines compared with the perpendicular wavelength ($k_\perp \gg k_\parallel$). Such examples are low-frequency drift instabilities, trapped-particle instabilities, lower hybrid waves, and the hydromagnetic instabilities including kink, tearing and Alfvén modes. This fact suggests that when simulating these phenomena, one need not keep very many grid points in the axial direction. In fact, the variation along the field lines is very slow compared with that in the cross section and therefore keeping only a reasonable number of the long-wavelength modes in the axial direction should be sufficient. This naturally suggests a new type of simulation model using a normal mode expansion in place of a spatial grid in the axial direction, while using the standard grid expansion in a two-dimensional cross section. As will be shown this model is quite useful for simulating realistic plasmas using presently available computers. It may be necessary, depending on the problems investigated, to build in a collision operator through the Monte Carlo technique for random process. This will partially compensate the neglect of the short-wavelength fluctuations which are responsible for the collisional effects.

2. *Cylindrical Model*

Let us consider, as the first example, a three-dimensional slab model of a rectangular cross section shown in Fig. 1. A toroidal model is considered later. Assume a particle has a finite size given by the Gaussian charge density [9]

$$\rho_j(x, y, z) = \frac{q_j}{(2\pi)^{3/2}a_x a_y a_z} \exp\left[-\left(\frac{(x - x_j)^2}{2a_x^2} + \frac{(y - y_j)^2}{2a_y^2} + \frac{(z - z_j)^2}{2a_z^2}\right)\right] \quad (1)$$

where (x_j, y_j, z_j) is the location of the center of the jth particle, q_j is its total charge, and a_x, a_y, and a_z are the particle size in three directions. We consider an electrostatic field only in this paper, although the extension to include the fully electromagnetic or magnetostatic interactions is straightforward.

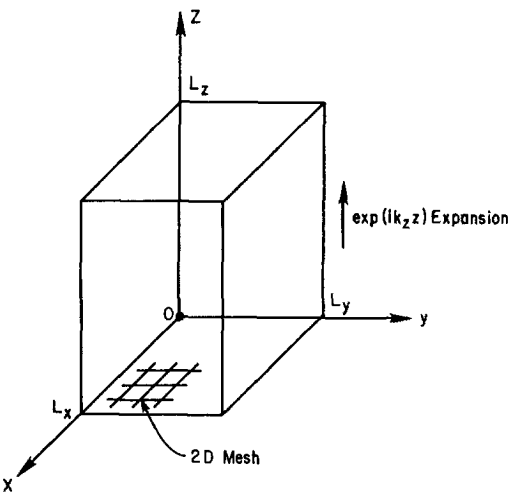

FIG. 1. A sketch for the three-dimensional slab model. Spatial grid is used in the x–y plane while the mode expansion is employed in the z-direction.

The Poisson equation for the electrostatic field would then be

$$\nabla^2\phi = -4\pi \sum_j \frac{q_j}{(2\pi)^{3/2}a_x a_y a_z} \exp\left[-\left(\frac{(x - x_j)^2}{2a_x^2} + \frac{(y - y_j)^2}{2a_y^2} + \frac{(z - z_j)^2}{2a_z^2}\right)\right]. \quad (2)$$

We will avoid the numerical difficulties arising from the use of the cylindrical coordinate throughout the paper, since we believe the Cartesian coordinate is much more superior to the cylindrical one in many aspects for numerical computations.

As described in the previous section, let us expand ϕ in terms of eigenfunctions which are simply $\exp(ik_z z)$ for the cylindrical model where $k_z = 2\pi n/L_z$. L_z is the length of the system which is assumed periodic in z.

$$\phi(x, y, z) = \sum_{n=-N}^{N} \phi_n(x, y) \exp(i(2\pi nz/L_z)) \tag{3}$$

where N is the number of modes in z one would like to keep in the model.

Similarly the charge density $\rho(x, y, z)$ is expanded in the same manner,

$$\rho(x, y, z) = \sum_{n=-N}^{N} \rho_n(x, y) \exp(i(2\pi nz/L_z)) \tag{4}$$

where

$$\begin{aligned}\rho_n(x, y) &= \frac{1}{L_z} \int_0^{L_z} \rho(x, y, z) \exp\left(-i \frac{2\pi nz}{L_z}\right) dz \\ &= \frac{1}{2\pi a_x a_y L_z} \exp\left(\frac{-k_z^2 a_z^2}{2}\right) \sum_j q_j \exp\left[-\left(\frac{(x - x_j)^2}{2a_x^2} + \frac{(y - y_j)^2}{2a_y^2}\right)\right] \\ &\quad \times \exp(-ik_z z_j).\end{aligned} \tag{5}$$

The equation for $\phi_n(x, y)$ is then found from Eqs. (2)–(5).

$$[\nabla_{xy}^2 - (2\pi n/L_z)^2]\, \phi_n(x, y) = -4\pi\rho_n(x, y). \tag{6}$$

Equation (6) is basically the Poisson equation in two dimensions, which can be solved by means of the multipole expansion scheme around the nearest grid point using the fast Fourier transform (FFT) [9]. Let us outline, for the sake of completeness, the multipole expansion method briefly here.

Let us first Fourier transform Eq. (6) with respect to x and y coordinates. Assuming a periodic boundary conditions in both x and y, we find

$$-[(k_x^2 + k_y^2) + (2\pi n/L_z)^2]\, \bar{\phi}_n(k_x, k_y) = -4\pi\bar{\rho}_n(k_x, k_y)$$

where

$$\begin{aligned}\bar{\rho}_n(k_x, k_y) &= \frac{1}{L_x L_y} \int_0^{L_x} \int_0^{L_y} \rho_n(x, y) \exp[-i(k_x x + k_y y)]\, dx\, dy \\ &= \frac{1}{L_x L_y L_z} \exp[-(k_x^2 a_x^2 + k_y^2 a_y^2 + k_z^2 a_z^2)/2] \sum_j q_j \\ &\quad \times \exp[-i(k_z z_j + k_x x_j + k_y y_j)].\end{aligned} \tag{7}$$

Here $k_x = 2\pi l/L_x$ and $k_y = 2\pi m/L_y$.

Introducing a two-dimensional spatial grid in the x–y plane, we expand (x_j, y_j) around its nearest grid point, i.e., $x_j = n_j^x \Delta + \delta x_j$, $y_j = n_j^y \Delta + \delta y_j$ where (n_j^x, n_j^y) is the nearest grid point of the jth particle and $(\delta x_j, \delta y_j)$ are the displacments from the nearest grid point.

According to the multipole expansion method, we expand $\exp(-ik_x x_j) = \exp(-ik_x n_j^x \Delta)(1 - ik_x \delta x_j)$ and $\exp(-ik_y y_j) = \exp(-ik_y n_j^y \Delta)(1 - ik_y \delta y_j)$ keeping up

to the dipole moments for each particle. We will keep the $\exp(-ik_z z_j)$ term unexpanded here because there is no grid in the z direction. Then $\bar{\rho}_n(k_x, k_y)$ would then be

$$\bar{\rho}_n(k_x, k_y, k_z) = \frac{1}{L_x L_y L_z} \exp[-(k_x^2 a_x^2 + k_y^2 a_y^2 + k_z^2 a_z^2)/2] \sum_{s=1}^{L_x} \sum_{s'=1}^{L_y} \times (\rho_{ss'} - ik_x \delta\rho^x_{ss'} - ik_y \delta\rho^y_{ss'}) \exp\left[-i2\pi\left(\frac{sl}{L_x} + \frac{s'm}{L_y}\right)\right] \tag{8}$$

where $\rho_{ss'}$ and $\delta\rho^x_{ss'}$, $\delta\rho^y_{ss'}$ are the monopole and the dipole charge densities at the (s, s') grid point weighted by the eigenfunction $\exp(-ik_z z_j)$. They are defined by

$$\rho_{ss'} = \sum_j q_j \exp(-ik_z z_j)\, U(s\Delta - x_j)\, U(s'\Delta - y_j),$$

$$\delta\rho^x_{ss'} = \sum_j q_j \exp(-ik_z z_j)(x_j - s\Delta)\, U(s\Delta - x_j)\, U(s'\Delta - y_j),$$

and

$$\delta\rho^y_{ss'} = \sum_j q_j \exp(-ik_z z_j)(y_j - s'\Delta)\, U(s\Delta - x_j)\, U(s'\Delta - y_j)$$

where

$$U(x - x_j) = 1 \quad \text{for} \quad |x - x_j| < \Delta/2,$$
$$= 0 \quad \text{for} \quad |x - x_j| > \Delta/2,$$

and the summation j is over all the particles. Here L_x and L_y are the length of the system in x and y in terms of the grid size Δ and therefore they correspond to the total number of grid points in each direction. It is clear that the double summation on the right-hand side of Eq. (8) is the two-dimensional fast Fourier transform of the weighted monopole and dipole charge densities on the grid points. It is straightforward to find the potential $\phi_n(x, y)$ by the inverse fast Fourier transform of $\phi_n(k_x, k_y)$ with respect to (k_x, k_y), i.e.,

$$\phi_n(s\Delta, s'\Delta) = \sum_{l=1}^{L_x} \sum_{l'=1}^{L_y} \phi_n(k_x, k_y) \exp\left[i2\pi\left(\frac{sl}{L_x} + \frac{s'l'}{L_y}\right)\right].$$

Finally the total potential will be given by summing over n as given by Eq. (3).

It is clear that the simulation method described above takes full advantage of both multipole expansion method in terms of finite-size particles combined with the fast Fourier transform technique on a spatial grid and the eigenfunction expansion method in the axial direction, which is much longer than the transverse dimension and would be too long to be represented in terms of a spatial grid.

Let us now calculate the force on a finite-size particle which is necessary in the equation of motion [9]. The electric field force on the jth particle will be given by

$$\mathbf{F}(x_j, y_j, z_j) = q_j \int \mathbf{E}(x, y, z) \frac{1}{(2\pi)^{3/2} a_x a_y a_z} \times \exp\left[-\left(\frac{(x - x_j)^2}{2a_x^2} + \frac{(y - y_j)^2}{2a_y^2} + \frac{(z - z_j)^2}{2a_z^2}\right)\right] dx\, dy\, dz \tag{9}$$

where $\mathbf{E}$ is calculated from ϕ and is assumed to take the form of

$$\mathbf{E}(x, y, z) = \sum_{n=-N}^{N} \mathbf{E}_n(x, y) \exp(-2\pi i n z/L_z).$$

The z integration can be carried out to find for the force in the x-direction

$$F_x(x_j, y_j, z_j) = \frac{q_j}{2\pi a_x a_y} \sum_{n=-N}^{N} \exp\left(\frac{-k_z^2 a_z^2}{2}\right) \exp(ik_z z_j) \iint E_{nx}(x, y)$$

$$\times \exp\left[-\left(\frac{(x - x_j)^2}{2a_x^2} + \frac{(y - y_j)^2}{2a_y^2}\right)\right] dx\, dy.$$

According to the procedure of multipole expansion scheme [9], F_x is now Fourier transformed with respect to x_j and y_j. Then

$$F_x(k_x, k_y, z_j) = q_j \sum_{n=-N}^{N} \exp\left(\frac{-k_z^2 a_z^2}{2}\right) \exp(ik_z z_j)\, E_{nx}(k_x, k_y)$$

$$\times \exp[-(k_x^2 a_x^2 + k_y^2 a_z^2)/2]. \tag{10}$$

$F_x(x_j, y_j, z_j)$ is calculated from the inverse fast Fourier transform of (10) and is expanded at around the nearest grid point, that is

$$F_x(x_j, y_j, z_j) = F_x(n_j^x \Delta, n_j^y \Delta, Z_j) + \delta x_j \frac{\partial F_x}{\partial x} + \delta y_j \frac{\partial F_x}{\partial y}$$

keeping up to the dipole terms. The derivatives of F_x are evaluated at the nearest grid point and are calculated by differencing F_x's on the neighboring points.

In the actual simulations, ions are pushed using the full Lorentz force while the electrons are assumed being guiding center particles. The standard predictor–corrector scheme is used for the electron orbit integration to keep the higher order of accuracy [6]. Furthermore, a modified version of dipole expansion, subtracted dipole, is used for all the simulations to reduce the required memory [9]. As will be shown in Section 3, the model works successfully to produce the expected thermal spectrum. For practical purposes, it is important to use a sausage-shape particle elongated in the axial direction ($a_z \gg a_x, a_y$) since it will naturally suppress the short-wavelength fluctuations in the axial direction neglected in the model.

It should be pointed out that since the model does not use a spatial grid in the axial direction, fast Fourier transform is not applicable in that direction. On the other hand, since the number of modes in the axial direction kept in the model is typically $N =$ 5–10, the code is not much slower than the conventional two-dimensional code as shown in Section 4.

3. *Toroidal Model*

After studying the new model for the cylindrical system, let us now consider a toroidal application. Consider a torus of rectangular cross section as shown in Fig. 2. The Poisson equation in this coordinate takes the form of

$$\frac{\partial^2 \Phi}{\partial r^2} + \frac{1}{r}\frac{\partial \Phi}{\partial r} + \frac{1}{r^2}\frac{\partial^2 \Phi}{\partial \phi^2} + \frac{\partial^2 \Phi}{\partial z^2} = -4\pi\rho(r, \phi, z) \tag{11}$$

where $\Phi(r, \phi, z)$ is the electrostatic potential and is usually assumed to vanish on the surrounding conducting wall. We will solve this equation by expanding the potential and charge density in terms of the eigenfunction in ϕ and the multipole expansion around the nearest grid point on the rectangular grid introduced in the poloidal cross section as before.

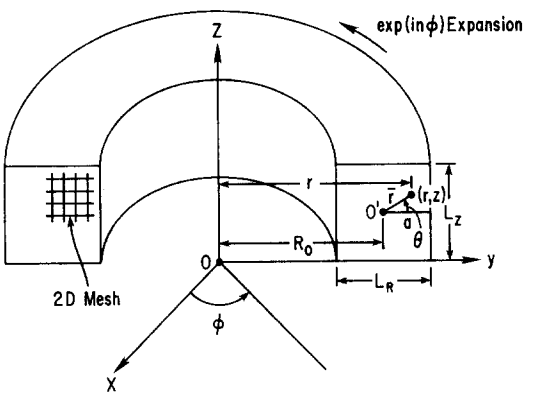

FIG. 2. A sketch for the toroidal model in the rectangular cross section. Note the coordinate chosen in the model.

Now expanding Φ and ρ in the toroidal direction,

$$\Phi(r, \phi, z) = \sum_{n=-N}^{N} \Phi_n(r, z) \exp(in\phi),$$

$$\rho(r, \phi, z) = \sum_{n=-N}^{N} \rho_n(r, z) \exp(in\phi).$$

Equation (11) is reduced to

$$\frac{\partial^2 \Phi_n}{\partial r^2} + \frac{1}{r}\frac{\partial \Phi_n}{\partial r} - \frac{n^2}{r^2}\Phi_n + \frac{\partial^2 \Phi_n}{\partial z^2} = -4\pi\rho_n . \tag{12}$$

To see how the multipole expansion method works for the toroidal system, let us Fourier transform the charge density with respect to ϕ first. Assuming a particle has a gaussian charge density in the cylindrical coordinate,

$$\rho_j(r, \phi, z) = \frac{q_j}{(2\pi)^{3/2} a_z a_r r_j a_\phi} \exp\left[-\left(\frac{(r - r_j)^2}{2a_r^2} + \frac{(\phi - \phi_j)^2}{2a_\phi^2} + \frac{(z - z_j)^2}{2a_z^2}\right)\right] \tag{13}$$

then

$$\begin{aligned}\rho_n(r, z) &= \frac{1}{2\pi} \int_0^{2\pi} \rho(r, \phi, z) e^{-in\phi}\, d\phi \\ &= \frac{\exp(-n^2 a_\phi^2/2)}{(2\pi)^2 a_r a_z} \sum_j \frac{q_j}{r_j} \exp[-(r - r_j)^2/2a_r^2 - (z - z_j)^2/2a_z^2 - in\phi_j]\end{aligned}$$

where a_r, a_ϕ, and a_z are the particle size in the (r, ϕ, z) coordinate. Note that the higher toroidal mode is effectively shielded as $\exp(-n^2 a_\phi^2/2)$.

Fourier transforming $\rho_n(r, z)$ with respect to z, we find

$$\begin{aligned}\rho_n(r, k_z) &= \frac{1}{L_z} \int_0^{L_z} \rho_n(r, z) \exp(-ik_z z)\, dz \\ &= \frac{\exp(-k_z^2 a_z^2/2 - n^2 a_\phi^2/2)}{(2\pi)^{3/2} a_r L_z} \sum_j \frac{q_j}{r_j} \exp[-i(n\phi_j + k_z z)] \exp[-(r - r_j)^2/2a_r^2].\end{aligned}$$

We note immediately that the fast Fourier transform may be employed in the z-direction. Writing $z_j = n_j^z \Delta z + \delta z_j$ where n_j^z is the nearest grid point in z for the jth particle, we find

$$\begin{aligned}\rho_n(r, k_z) = \frac{\exp(-k_z^2 a_z^2/2 - n^2 a_\phi^2/2)}{(2\pi)^{3/2} a_r L_z} &\sum_j q_j \exp[-i(n\phi_j + k_z n_j^z \Delta z)] (1 - ik_z\, \delta z_j) \\ &\times \exp[-(r - r_j)^2/2a_r^2] \frac{1}{r_j}.\end{aligned} \tag{14}$$

Finally we note in the r direction, the fast Fourier transform may not be appropriate since the system, Eq. (12), is aperiodic in the radial direction and obviously the trigonometric functions are not the eigenfunctions. Therefore, instead of using the fast Fourier transforms, we solve Eq. (12) by means of a spline method as described later. However, to determine the charge density on the radial grid in terms of the multipole expansion method, we will use the fast Fourier transform. Since the charge density and the potential vanish at the boundaries at $r = R_1$ and R_2, we will consider the system periodic.

Fourier transforming $\rho_n(r, k_z)$ with respect to r, we find

$$\begin{aligned}\bar{\rho}_n(k_r, k_z) &= \frac{1}{L_R} \int_0^{L_R} \rho_n(R_1 + s, k_z) \exp(-ik_r s)\, ds \\ &= \frac{\exp(-k_z^2 a_z^2/2 - n^2 a_\phi^2/2)}{2\pi L_R L_z} \sum_j q_j \exp[-i(n\phi_j + k_z n_j^z \Delta z)] (1 - ik_z\, \delta z_j) \\ &\cdot \frac{1}{(2\pi)^{1/2} a_r} \int_{-\infty}^{\infty} \exp[-(r - r_j)^2/2a_r^2 - ik_r(r - R_1)] \frac{d(r - r_j)}{r_j}.\end{aligned} \tag{15}$$

The r integral may be carried out easily to find

$$I_{kr} \equiv \frac{1}{(2\pi)^{1/2}a_r}\int_{-\infty}^{\infty}\frac{\exp[-(r-r_j)^2/2a_r^2]}{r_j}\exp[-ik_r(r-R_1)]\,d(r-r_j)$$
$$= \frac{\exp[(-k_r^2a_r^2)/2]}{r_j}\exp[-ik_r(r_j-R_1)].$$

Introducing a radial grid with the uniform width Δr, $r_j = R_1 + n_j^r\Delta r + \delta r_j$ and keeping only up to the dipole term, I_{kr} becomes

$$I_{kr} = \frac{\exp(-k_r^2a_r^2/2)}{r_j}\exp(-ik_rn_j^r\,\Delta r)\,(1 - ik_r\,\delta r_j). \tag{16}$$

Then $\bar{\rho}_n(k_r, k_z)$ becomes

$$\bar{\rho}_n(k_r, k_z) = \frac{\exp[-(k_z^2a_z^2 + k_r^2a_r^2 + n^2a_\phi^2)/2]}{L_RL_z2\pi}\sum_{s=1}^{L_z}\sum_{s'=1}^{L_R}$$
$$= \frac{(\rho_{ss'} - ik_r\,\delta\rho^r_{ss'} - ik_z\,\delta\rho^z_{ss'})}{r_{s'}}\exp(-i2\pi sl/L_z)$$
$$\cdot\ \exp(-i2\pi s'l'/L_R) \tag{17}$$

where $k_z = 2\pi l/L_z$, $k_r = 2\pi l'/L_R$, and $\rho_{ss'}$ and $\delta\rho^{z,r}_{ss'}$ are the nearest grid point and the dipole charge contributions at the grid point (s, s') weighted by the $\exp(-in\phi_j)$ defined by

$$\rho_{ss'} = \sum_j q_j\exp(-in\phi_j)\,U(s\Delta z - z_j)\,U(R_1 + s'\Delta r - r_j),$$

$$\delta\rho^z_{ss'} = \sum_j q_j\exp(-in\phi_j)\,(z_j - s\Delta z)\,U(s\Delta z - z_j)\,U(R_1 + s'\Delta r - r_j),$$

and

$$\delta\rho^r_{ss'} = \sum_j q_j\exp(-in\phi_j)\,(r_j - R_1 - s'\Delta r)\,U(s\Delta z - z_j)\,U(R_1 + s'\Delta r - r_j).$$

Note that we have approximated $r_j = r_{s'}[1 + O(\delta r_j/r_j)]$ and $\delta r_j/r_j$ is smaller than the dipole term by the aspect ratio. In Eq. (17) the expansion of the finite-size particles up to the dipole moment about the nearest grid point has been carried out both in z and r directions using an $(r - z)$ rectangular mesh, while in the toroidal direction, no expansion is made and the eigenfunction $\exp(-in\phi)$ is used all the way keeping the reasonable number of modes in that direction.

Inverting the finite Fourier transform of $\bar{\rho}_n(k_r, k_z)$, with respect to k_r, we obtain the charge density on the radial grid points $\rho_n(R_1 + n^r\Delta r, k_z)$. The Poisson equation in r direction finally becomes

$$\left[\frac{d^2}{dr^2} + \frac{1}{r}\frac{d}{dr} - \left(\frac{n^2}{r^2} + k_z^2\right)\right]\Phi_n(r, k_z) = -4\pi\rho_n(r, k_z) \tag{18}$$

where $\rho_n(r,k_z)$ is calculated by inverting Eq. (17) numerically. Radial Eq. (18) has been solved by using the cubic spline technique as described below [15, 16]. Cubic spline has been applied successfully in integrating the nonlinear Vlasov equation [16].

Let f_i ($i = 1,\ldots, N$) be the values of a function f on N equally spaced grid points with a width Δ. Using cubic spline we write for the interpolation functions

$$y_i(r) = f_i + P_i \frac{(r - r_i)}{\Delta} + \frac{1}{2} S_i \frac{(r - r_i)^2}{\Delta^2} + g_i \frac{(r - r_i)^3}{\Delta^3} \tag{19}$$

where $r_{i-1} \leq r \leq r_{i+1}$. From the condition that the function and its derivatives are continuous at the grid points, it is easy to show that the recurrence formula for P_i's and S_i's are

$$3(f_i - f_{i+1}) + P_{i+1} + 2P_i + \tfrac{1}{2}S_i = 0 \tag{20}$$

and

$$P_{i-1} + 4P_i + P_{i+1} = 3(f_{i+1} - f_{i-1}) \tag{21}$$

where $\Delta = 1$ is assumed. From Eq. (19) we immediately see that P_i and S_i correspond to the values of $dy_i/dr\,|_{r=r_i}$ and $d^2y_i/dr^2\,|_{r=r_i}$, respectively. If we write radial Poisson Eq. (18) in a finite difference form and approximate the first and second derivatives of the potential by the spline values, Eq. (18) becomes

$$S_i + B_iP_i + C_if_i = \rho_i \tag{22}$$

where B_i, C_i are constant coefficients associated with Eq. (18) and ρ_i stands for the density on the radial mesh. Now eliminating S_i and P_i from Eqs. (20)–(22), we arrive at the final difference equation

$$\begin{aligned}
&\left(\frac{(B_i - 4)[2(C_{i-1} - 6) - 6(B_{i-1} - 4)]}{4 + (B_{i-1} - 4)(B_i + 4)}\right) f_{i-1} \\
&+ \left((C_i - 6) + \frac{(B_i - 4)[12 - (B_{i-1} - 4)(C_i - 6)]}{[4 + (B_{i-1} - 4)(B_i + 4)]} + \frac{2[6(B_i - 4) - 2(C_i - 6)]}{4 + (B_i - 4)(B_{i+1} + 4)}\right) f_i \\
&+ \left(6 - \frac{2[12 - (B_i - 4)(C_{i+1} - 6)]}{4 + (B_i - 4)(B_{i+1} + 4)}\right) f_{i+1} = \left(\frac{2(B_i - 4)}{4 + (B_{i-1} - 4)(B_i + 4)}\right) \rho_{i-1} \\
&+ \left(1 - \frac{(B_{i-1} - 4)(B_i - 4)}{4 + (B_{i-1} - 4)(B_i + 4)} - \frac{4}{4 + (B_i - 4)(B_{i+1} + 4}\right) \rho_i \\
&+ \left(\frac{2(B_i - 4)}{4 + (B_i - 4)(B_{i+1} + 4)}\right) \rho_{i+1}\,.
\end{aligned} \tag{23}$$

This equation can be solved with appropriate boundary conditions. The error analysis of spline has been given in many places [15] and is proportional to Δ^4. The above scheme has been tested for solving the Poisson equation where the solution is known analytically to be a Bessel function. The numerical results are found to agree with the analytic results within the sufficient accuracy.

Now let us briefly calculate the force on a finite-size particle. The electric force for a particle at (r_j, ϕ_j, z_j) is given by

$$\mathbf{F}(r_j, \phi_j, z_j) = q_j \int \mathbf{E}(r, \phi, z) \frac{1}{(2\pi)^{3/2} a_z a_r r_j a_\phi} \times \exp[-(r - r_j)^2/2a_r^2 - (z - z_j)^2/2a_z^2 - (\phi - \phi_j)^2/2a_\phi^2] r \, dr \, d\phi \, dz$$

where $\mathbf{E}(r, \phi, z)$ is calculated from $\Phi_n(k_r, k_z)$ and is given by, for example,

$$E_z(r, \phi, z) = \sum_{n=-N}^{N} E_n(r, z) \exp(in\phi)$$

then

$$F_z(r_j, \phi_j, z_j) = \sum_{n=-N}^{N} q_j \frac{\exp(-n^2 a_\phi^2/2) \cdot \exp(in\phi_j)}{2\pi a_r a_z} \int E_{nz}(r, z) \cdot \exp(-[(z - z_j)^2/2a_z^2 + (r - r_j)^2/2a_r^2]) \, dr \, dz.$$

Now following the procedure of multipole expansion scheme, let us Fourier transform the force $F_z(r_j, \phi_j, z_j)$ with respect to (r_j, z_j)

$$F_z(k_r, \phi_j, k_z) = \sum_{n=-N}^{N} \frac{q_j \cdot \exp(-n^2 a_\phi^2/2) \cdot \exp(in\phi_j)}{2\pi a_r a_z} \int dr \, dz \int_{R_1}^{R_2} dr_j \int_0^{L_z} dz_j \cdot \exp(-(z - z_j)^2/2a_z^2 - (r - r_j)^2/2a_r^2) \cdot \exp[-i(k_z z_j + k_r(r_j - R_1))] E_{nz}(r, z).$$

The integral with respect to z and z_j is straightforward in finding

$$F_z(k_r, \phi_j, k_z) = \frac{\exp(-k_z^2 a_z^2/2 - n^2 a_\phi^2/2)}{(2\pi)^{1/2} a_r} \sum_{n=-N}^{N} q_j \exp(in\phi_j) \int dr \int_{R_1}^{R_2} dr_j E_{nz}(r, k_z) \cdot \exp(-(r - r_j)^2/2a_r^2) \exp(-ik_r(r_j - R_1))$$

$$= \exp(-(k_z^2 a_z^2 + k_r^2 a_r^2 + n^2 a_\phi^2)/2) \sum_{n=-N}^{N} q_j \exp(in\phi_j) E_{nz}(k_r, k_z). \quad (24)$$

The force on the jth particle is calculated from the inverse transforms of (24) and then expanded around the nearest grid point. Writing $r_j = n_j^r \Delta r + \delta r_j$ and $z_j = n_j^z \Delta z + \delta z_j$,

$$F_z(r_j, \phi_j, z_j) = F_z(n_j^r \Delta r, \phi_j, n_j^z \Delta z) + \delta r_j \frac{\partial F_r}{\partial r} + \delta z_j \frac{\partial F_r}{\partial z}$$

where the derivatives of F_z are evaluated at the nearest grid point and are calculated by differencing F_z's on the neighboring points.

The evolution of the system is obtained by pushing ions with the full Lorentz force and integrating the guiding center drift equations for electrons. The electron guiding center equations are given by

$$\frac{d\mathbf{r}}{dt} = \frac{(\mathbf{v}\cdot\mathbf{B})}{B^2}\mathbf{B} + \frac{c\mathbf{E}\times\mathbf{B}}{B^2} - \frac{1}{\Omega_e B^2}\left(\frac{\mu B}{m_e} + v_\parallel{}^2\right)\mathbf{B}\times\nabla B,$$

$$\frac{dv_\parallel}{dt} = -\frac{q}{m_e}\frac{\mathbf{E}\cdot\mathbf{B}}{B} - \frac{1}{m_e B}\mathbf{B}\cdot\nabla(\mu B) + \frac{cv_\parallel}{B^3}(\mathbf{E}\times\mathbf{B})\cdot\nabla B,$$

$$\mu = \frac{mv_\perp{}^2}{2B} = \text{constant}, \tag{25}$$

where

$$v_\parallel = \frac{\mathbf{v}\cdot\mathbf{B}}{B} \quad \text{and} \quad \Omega_e = \frac{eB}{m_e c}.$$

The integration scheme used is a second-order predictor–corrector scheme known as the modified Euler method [17]. Symbolically, the guiding center equation can be written as $d\mathbf{r}/dt = \mathbf{v}(\mathbf{r}, t)$. Then the time difference scheme is

$$\bar{\mathbf{r}}_{n+1} = \mathbf{r}_{n-1} + 2\Delta t\,\mathbf{v}(\mathbf{r}_n, t_n),$$
$$\mathbf{r}_{n+1} = \mathbf{r}_n + \Delta t/2(\mathbf{v}(\mathbf{r}_n, t_n) + \mathbf{v}(\bar{\mathbf{r}}_{n+1}, t_{n+1})). \tag{26}$$

Note that this scheme requires two solutions of the Poisson equation per time step.

3. Test of the Model

After developing the cylindrical and toroidal models described above, we have tested the codes by measuring the total energy conservation, thermal fluctuation spectrum, and the particle orbit.

1. *Test of the Cylindrical Model*

Let us briefly describe the test results from the three-dimensional slab model. We consider a simple system in which the magnetic field is uniform and in the z-direction only. The plasma is assumed uniform and is periodic in y- and z-directions while it is bounded between $x = 0$ and L_x due to the conducting walls which reflect particles in the same manner described in Ref. [6].

Figure 3 shows the time-averaged thermal spectrum for different modes of $\mathbf{k} = (k_x, k_y, k_z) = (2\pi m/L_x, 2\pi n/L_y, 2\pi l/L_z)$ where the size of the box was chosen $(L_x, L_y, L_z) = (32, 32, 32)$. In this particular example, 5 modes ($l = 0, \pm1, \pm2, \pm3, \pm4$) in the z-direction while 32×32 spatial mesh was employed in the x–y plane. The other parameters of simulations are 2^{12} particles for ions and electrons respectively, $\Omega_e/\omega_{pe} = 5$, $T_e = T_i$, $m_i/m_e = 25$, $v_e = 2$, $a_x = a_y = a_z = 1$, and $\omega_{pe}\Delta t = 1$.

Ω_e is the electron gyrofrequency, v_e is the electron thermal speed, a is the Gaussian particle size which is taken isotropic in three directions, and Δt is the time integration step size. We note that the fluctuation spectrum averaged over $\omega_{pe}t = 0$–50 is in good agreement with the theoretical prediction $E_k^2/8\pi = T/2\ [1]/[1 + k^2\lambda_D^2 \exp(k^2a^2)]$ as shown by the solid line. The total energy conservation was about 0.5% at the end of the calculation. This may be due to, for example, too large a time step of integration or too few particles per Debye sphere. Electrons were pushed by the quiding center drift equation in the transverse direction while the electron parallel motion was followed exactly. Ions were pushed exactly. Full dipole calculations were employed in this example which took about 100 μsec per particle for one iteration on the CDC 7600 using a Fortran code utilizing Stacklib subroutines. The nearest grid point calculations take 60 μsec and it may be required for large, three-dimensional calculations to be finished within a reasonable computing time.

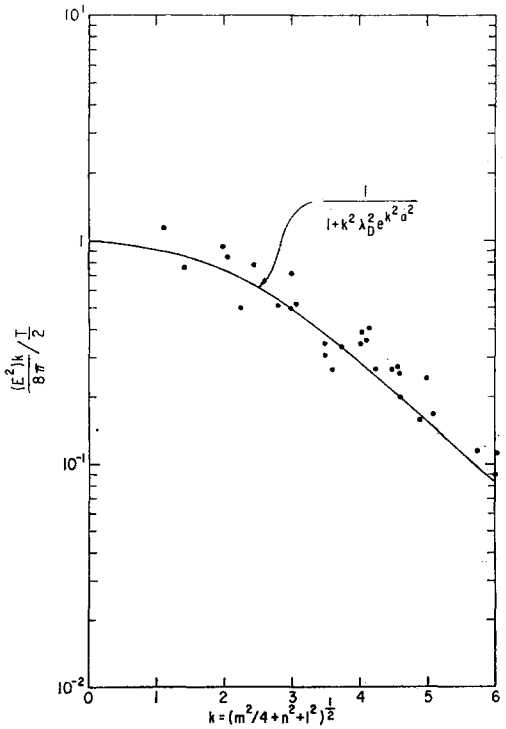

FIG. 3. Fluctuation spectrum for the three-dimensional slab model described in the text. The time-averaged simulation result agrees well with the theoretical predictions.

We have simulated the same example shown above with the number of modes in z doubled ($l = 0, \pm1, \pm2, \ldots, \pm9$). It is observed that the shorter-wavelength modes also satisfy the energy partition law as well. There was no significant differences

observed for the gross behavior of plasmas such as total energy conservation for both cases. This is an encouraging observation since it indicates that we need not keep many modes in the axial direction.

Several production runs have been carried out after testing the model. Typically the system size is 64×64 grid in the x–y plane and 1280 in the z-direction with 2^{18} particles. $M_i/M_e = 100$, $\omega_{pe}\Delta t = 4$, $\Omega_e/\omega_{pe} = 5$, $T_e/T_i = 4$, $a_x = a_y = 2$, $a_z = 64$, and $v_e = 2$ were used. We have observed low-frequency drift wave instabilities and anomalous diffusion. In this example, four modes were kept in the z direction and it took 5–6 hours to reach the nonlinear saturation state.

2. *Test of the Toroidal Model*

In the toroidal model the imposed magnetic field is taken to be $\mathbf{B} = \hat{e}_\theta B_\theta + \hat{e}_\phi B_\phi$, where

$$B_\phi(r) = B_\phi^{(0)} R_0/r,$$

$$B_\theta = \bar{r}B_\phi^{(0)}/q(\bar{r})\, R_0 = \frac{\bar{r}B_\phi^{(0)}}{q^{(0)}R_0}\left(1 - \frac{\bar{r}^2}{2\bar{a}^2}\right),$$

and

$$r = R_0 + \bar{r}\cos\theta.$$

The coordinate $(\bar{r}, \theta)$ measures the position in the cross-sectional plane of the torus with $\bar{r}$ the distance from the minor axis and θ measured from the toroidal plane to the inside. R_0 and $\bar{a}$ are the major and minor radius, respectively, and $q^{(0)}$ is the safety factor and $B_\phi^{(0)}$ the toroidal field at the minor radius. The plasma is assumed to be bounded due to the conducting walls which reflect particles.

Initially the plasma density and temperature profiles are taken to be gaussians with, e.g.,

$$n(\bar{r}) = \frac{2e^{-r^2/C\bar{a}^2}}{C\bar{a}^2(1 - e^{-1/C})}.$$

The constant C characterizes the degree of nonuniformity. The plasma is locally Maxwellian. Figure 4 shows the fluctuation spectrum averaged over the r-direction for different modes of $(k_z, k_\phi) = (2\pi l/L_z, n/R_0)$. The size of the torus is taken $\bar{a} = 16$, $R_0 = 40$. There are five modes ($n = 0, \pm1, \pm2, \pm3, \pm4$) in the toroidal direction ϕ and 32×32 spatial mesh was employed in the r–z cross-sectional plane. The other parameters of the run are 2^{14} particles for each species, $\Omega_e/\omega_{pe} = 4$, $T_e/T_i = 10$, $m_i/m_e = 100$, $\lambda_{De} = 2$, a (isotropic particle size) $= 1$ and $\omega_{pe}\Delta t = 1$, $C_{Ti} = C_{Te} = 0.25$, $C_{ni} = C_{ne} = 0.5$, where Ω_e is the electron gyrofrequency at the minor radius, ω_{pe} is the average electron plasma frequency, C_T and C_n denote

temperature and density nonuniformity, and $T_e/T_i = 10$ at the center of minor radius.

As we can see, the agreement between the theoretical predictions and the numerical results averaged over $\omega_{pe}t = 50$–100 is quite satisfactory for short-wavelength modes. The long-wavelength modes generated by the ∇B drift of the ions have not yet reached the equilibrium, because the computations were too short for the electron flow along the field lines to compensate the ions. The theoretical fluctuation spectrum averaged over the radial direction for a finite-size particle system is given by

$$\int r\,dr\,\frac{|E(r, n, l)|^2}{8\pi}\Big/\left(\frac{T}{2}L_R\right) = \frac{1}{2\pi\lambda_D}\int_0^{\pi\lambda_D}\frac{dx}{1+(y^2+x^2)\exp[(y^2+x^2)\,a^2/\lambda_D{}^2]}$$

where $y^2 = (n^2/R_0{}^2 + l^2\Delta k_z{}^2)\lambda_D{}^2$ and is shown by the solid line. The error for the total energy conservation at the end of the calculation ($\omega_{pe}t = 100$) is about 1 %.

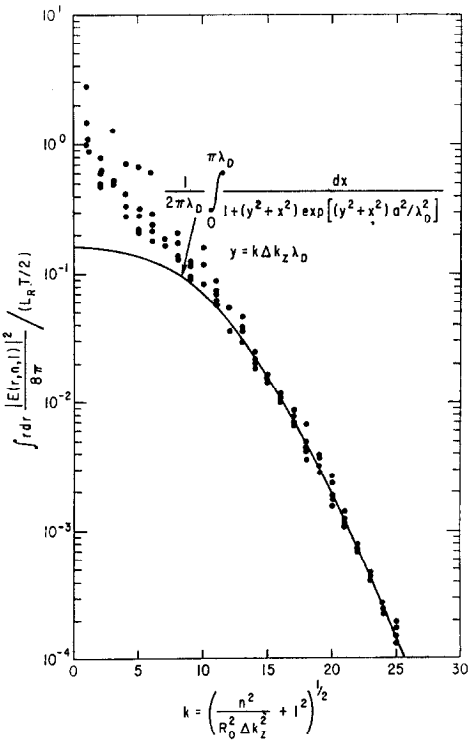

FIG. 4. Fluctuation spectrum averaged over the radial direction for the toroidal model described in the text. The time-averaged simulation result agrees well with the theoretical prediction shown by the solid line. The enhancement for long-wavelength modes is presumably due to the ∇B drift which separates the ions from the electrons in the z-directions.

This may be due to too large a time step of integration, too few particles per Debye sphere, the reflecting boundary walls which exert external force on the particles. Because the toroidal model is more complicated than the slab model, the former takes about 50 % more computations than the latter.

4. Concluding Remarks

We have developed a new class of three-dimensional simulation models for cylindrical and toroidal geometry by employing a hybrid approach of eigenfunction expansion and the multipole expansion on a spatial grid. The model is particularly useful for a system in which the axial length is much longer than the transverse dimension as seen for most of the experimental device for controlled fusion such as a tokamak, stellarator, and a z-pinch.

Preliminary results for the test of the models are quite satisfactory and are encouraging for the application to more realistic problems. Full three-dimensional simulations for the drift-wave and trapped-particle instabilities are now studied by extending the previous slab model [6, 18].

The other important area in which the model described may be very useful is the low-frequency hydromagnetic behavior of a plasma in cylindrical and toroidal systems from the microscopic point of view. In particular, king-tearing modes may be conveniently simulated by keeping several modes in the toroidal direction such as seen for the tokamak experiments. The present model is quite general including most of the kinetic effects in contrast to fluid model so that, for example, the effects of the plasma transport on the stability is automatically included in a self-consistent manner. It is, of course, necessary to build in the self-consistent magnetic field, in addition to the electrostatic electric field. While the present code is collisionless, the collisional effects may be added in terms of Monte Carlo method [4].

In the toroidal model, the charge density of a finite-size particle, Eq. (13), depends on the radial position r_j through the geometric factor $1/r_j$. However, since the shielding of the toroidal modes is due to $\exp(-n^2 a_b^2/2)$, which is independent of the geometric factor, the short-wavelength modes comparable to the particle size in the toroidal direction are strongly shielded and, therefore, have no effects on the dynamics of the system.

One other remark is ready for the method we developed for the simulation of toroidal plasmas. Because of the finite size of the particles, we calculated the grid charge density by Fourier transforming the exact charge density and then kept it up to the dipole term. Then the grid charge density was transformed back to physical space with respect to the radial coordinate since the Poisson equation was solved on the radial mesh points by means of spline technique. This potential had to be transformed to k_r space to calculate the force on a particle up to the dipole term. It is clear that if we could solve the radial Poisson equation in the transformed space rather than the physical mesh points, then two one-dimensional transforms would be saved. One obvious candidate is to make use of the Hankel (Bessel) transform

[19] in the radial direction instead of the Fourier transform since the Bessel function is the eigenfunction of the Poisson equation given by (18). We are investigating this alternate method as well and the results will be reported elsewhere.

ACKNOWLEDGMENT

This work was supported by the United States Energy Research and Development Administration contract E(11-1)-3073.

REFERENCES

1. O. BUNEMAN, *Phys. Rev. Lett.* **115** (1959), 503.
2. J. M. DAWSON, *Phys. Fluids* **5** (1962), 445.
3. K. TSANG, Y. MATSUDA AND H. OKUDA, *Phys. Fluids* **18** (1975), 1282.
4. Y. MATSUDA, J. SAMPSON AND H. OKUDA, "Proceedings of Annual Meeting on Theoretical Aspects of Controlled Thermonuclear Research, Madison, Wisconsin (April 1976)," paper 2A-13.
5. R. V. JENSEN, S. A. COHEN, Y. MATSUDA AND H. OKUDA, *Bull. Amer. Phys. Soc.* **20** (1975), paper 6H11, 1330.
6. W. W. LEE AND H. OKUDA, *J. Computational Phys.* to appear; Princeton Plasma Physics Laboratory MATT-1231.
7. A. HASEGAWA AND H. OKUDA, *Phys. Fluids* **11** (1968), 1995.
8. C. K. BIRDSALL AND D. FUSS, *J. Computational Phys.* **3** (1969), 494; R. L. MORSE AND C. W. NIELSON, *Phys. Fluids* **12** (1969), 2418.
9. W. L. KRUER, J. M. DAWSON, AND B. ROSEN, *J. Computational Phys.* **13** (1973), 114; L. CHEN AND H. OKUDA, *J. Computational Phys.* **19** (1975), 339.
10. R. L. MORSE AND C. W. NIELSON, *Phys. Rev. Lett.* **23** (1969), 1087; D. BISKAMP, K. VON HAGENOW AND H. WELTER, *Phys. Rev. Lett. A* **39** (1972), 351.
11. H. OKUDA AND J. M. DAWSON, *Phys. Rev. Lett.* **28** (1972), 408.
12. E. L. LINDMAN, *J. Computational Phys.* **5** (1970), 13.
13. A. B. LANGDON, *J. Computational Phys.* **6** (1970), 247.
14. See, for example, Princeton Q-1 device, N. RYNN, *Rev. Sci. Instr.* **35** (1964), 40.
15. F. B. HILDEBRAND, "Introduction to Numerical Analysis," 2nd ed., Chapter 9, McGraw–Hill, New York, 1974.
16. C. Z. CHENG AND G. KNORR, *J. Computational Phys.* **22** (1976), 330.
17. R. W. HAMMING, "Introduction to Applied Numerical Analysis," Chapter 3, McGraw–Hill, New York, 1973.
18. Y. MATSUDA AND H. OKUDA, *Phys. Rev. Lett.* **36** (1976), 474.
19. C. J. TRANTER, "Integral Transforms in Mathematical Physics," p. 11, Wiley, New York, 1965.